

Eigenmodes in an ultra-relativistic ultra-magnetized pair QED-plasma

 Ryan T. Low¹ and  Mikhail V. Medvedev^{1,2}

¹⁾Department of Physics and Astronomy, University of Kansas, Lawrence, KS 66045

²⁾Laboratory for Nuclear Science, Massachusetts Institute of Technology, Cambridge, MA 02139

(*Electronic mail: rtlow@ku.edu)

Ultra-relativistic quantum-electrodynamic (QED) plasmas, characterized by magnetic field strengths approaching and even exceeding the Schwinger field of approximately $B_Q \approx 4 \times 10^{13}$ gauss, hold significant interest for laser-plasma experiments and astrophysical observations of neutron stars and magnetars. In this study, we investigate the joint modification of normal plasma modes in ultra-relativistic electron-positron plasmas, both charge neutral and non-neutral, by the super-strong magnetic field and plasma relativistic temperature. Our analysis shows that the most substantial modification concerns the reduction of the plasma frequency cutoff, resulting in relativistic and field-induced transparency. Additionally, we observe a temperature-independent modification of the index of refraction of electromagnetic waves, which coincides with the behavior observed in a cold QED plasma.

I. INTRODUCTION

The study of plasma behavior in ultra-strong magnetic fields, particularly those approaching or even exceeding the Schwinger field strength $B_Q = m_e^2 c^2 / e \hbar \sim 4 \times 10^{13}$ gauss, represents a novel frontier in modern plasma research.

Existing and planned laser facilities, such as the Ultra-short Pulse Laser System (ZEUS), the Center for Relativistic Laser Science (CORELS), and the Laser Und XFEL Experiment (LUXE), are attempting to achieve field strengths and particle energies at which the quantum-electrodynamic (QED) effects become significant^{1–3}. However, the laser facilities primarily explore conditions in the weak field limit⁴, where the magnetic field strength is much less than the critical magnetic field strength, $B \ll B_Q$. In contrast, significantly stronger magnetic fields are present in nature. In particular, neutron stars can possess magnetic fields exceeding the Schwinger field and reaching $B_* \sim 10^{15}$ gauss and more. This category of neutron stars is designated as magnetars⁵. At QED field strengths Maxwell's equations become nonlinear, which leads to a wealth of interesting phenomena, such as, polarization-dependent vacuum index of refraction (vacuum birefringence), scattering of light by light, and three-photon interactions (photon splitting), including applications to neutron star magnetospheres^{6–11}. In the recent years, the QED effects were included in computational codes at the level of single-particle effects and are used, for instance, in modeling magnetic reconnection in ultra-strongly magnetized plasmas and the generation of QED cascades in laser plasmas^{12–15}, as well as in a general QED-plasma solver¹⁶.

Notably, however, the electromagnetic fields in magnetars and laser experiments are not vacuum fields. In contrast, the systems possess a substantial plasma component. In laser experiments, plasma is either created by the interaction with a target, or the e^\pm pair plasma can be created from the laser beam via the Breit-Wheeler process^{17,18}. In magnetars, the magnetosphere can be twisted by surface shear motions^{5,19}, so it is threaded by electric currents $\mathbf{j} = (c/4\pi)\nabla \times \mathbf{B}$. Thus, their magnetospheres carry electron-positron plasma needed to maintain the current, $n = j/ce \simeq 10^{17} B_{15} r_6^{-1} \text{ cm}^{-3}$, where $B_{15} = B/(10^{15} \text{ gauss})$ and $r_6 = r/(10^6 \text{ cm})$ is the radial distance from the center of the magnetar. Quite impor-

tantly, the magnetospheric plasma is not completely charge-neutral. In order to maintain corotation with the star (the magnetic field is anchored in the neutron star crust), the magnetosphere must locally contain plasma with a charge density at least equal to the “Goldreich-Julian” charge density, $\rho_{GJ} \approx \Omega_* \cdot \mathbf{B} / 2c$, where Ω_* is the angular velocity of the neutron star (magnetar) rotation. Note that the sign of the charge density varies throughout the magnetosphere depending on the angle between the magnetic field and the neutron star spin. The “Goldreich-Julian” particle density is $n_{GJ} = \rho_{GJ}/e \simeq (7 \times 10^{13} \text{ cm}^{-3}) B_{15}/P$, where $P = 2\pi/\Omega_*$ is the spin period of the magnetar or a neutron star in seconds. The ratio $\mathcal{M} = n/n_{GJ} \sim 10^3 r_6^{-1}$ is called the “multiplicity” and is related to the degree of non-neutrality of the magnetospheric plasma (see below). Finally, a neutron star (magnetar) crust is a conducting solid with free electrons, thus, it is also a magnetized purely electron plasma. The electron density varies between $n \sim 2.5 \times 10^{36} \text{ cm}^{-3}$ at the liquid core-solid crust interface and $n \sim 3 \times 10^{31} \text{ cm}^{-3}$ at the neutron star surface^{20,21}.

Paper I²² develops the QED-plasma framework, which incorporates the nonlinear QED-Maxwell equations into plasma dynamics. It also considers how the normal modes in a cold plasma ($k_B T \rightarrow 0$) are modified by QED effects. Here we extend the analysis to the case of relativistic plasma, which temperature is much larger than the particles' rest mass $k_B T \gg m_e c^2$.

The rest of the paper is organized as follows. Section II describes the linear wave formalism in a relativistic ultra-magnetized plasma and derives the corresponding dispersion relation. In Section III a comprehensive analytical analysis of the normal mode dispersion, their characteristic frequencies and relations is presented. Section IV presents the full numerical solution of the dispersion relation and identifies the corresponding branches. Their dependence on the field strength and temperature is illustrated. Section V summarizes essential results.

II. LINEAR WAVES

In this study, we employ the QED-plasma framework developed in Paper I²². This framework enables the investigation of the normal plasma modes, provided with the plasma electric susceptibility tensor, $\chi_{ij}^{\text{plasma}} = \epsilon_{ij} - \delta_{ij}$, where ϵ_{ij} is the plasma dielectric tensor. The reader is referred to Paper I for extensive details.

Consider a non-neutral ultrarelativistic pair plasma characterized by the non-neutrality parameter $\Delta n/n$, where $\Delta n = n^+ - n^-$ is the difference between the background positron and electron plasma densities, and $n_0 = n^+ + n^-$ is the total lepton density. We, however, assume that there are no net background currents associated with either species. We consider the case of strongly magnetized and magnetically dominated plasma, so that the cyclotron frequency is much larger than the electron plasma frequency, and the electron plasma frequency is much larger than the frequency of the considered wave modes.

In what follows, we denote $\omega_p = \sqrt{4\pi n e^2/m_e}$ the non-relativistic electron plasma frequency and $\Omega = eB/m_e c$ the non-relativistic electron cyclotron frequency. The electron gyroscale in a QED-strong magnetic field is negligibly small, $k_\perp^2 \rho_e^2 \ll 1$, because the electrons reach the lowest energy Landau level almost instantaneously. We conventionally choose the coordinate frame such that the wave vector is given by $\mathbf{k} = (k_\perp, 0, k_z)$, where z is the direction of the background magnetic field.

Under these assumptions, the plasma electric susceptibility tensor is given by expression^{22–24}:

$$\chi_{ij}^{\text{plasma}} = \begin{pmatrix} \chi_\perp & ig & 0 \\ -ig & \chi_\perp & 0 \\ 0 & 0 & \chi_\parallel \end{pmatrix}, \quad (1)$$

where

$$\chi_\perp = -\frac{\omega_p^2}{\omega^2 - \Omega^2}, \quad (2)$$

$$\chi_\parallel = -Q(\omega, \mathbf{k}), \quad (3)$$

$$g = -\frac{\omega_p^2 \Omega}{\omega(\omega^2 - \Omega^2)} \frac{\Delta n}{n}. \quad (4)$$

Note that the off-diagonal components $\pm ig$ are related to the breakdown of the charge neutrality. If we assume that n_{GJ} represent the entirely non-neutral fraction of the plasma, then the “non-neutrality fraction”, $\Delta n/n$, that will appear later can be approximated as the inverse multiplicity factor $\Delta n/n \sim n_{\text{GJ}}/n \sim \mathcal{M}^{-1}$.

In the above expressions, the function $Q(\omega, \mathbf{k})$ depends on the particle distribution function. It will be discussed below. Note the shape of the particle distribution and the thermal effects in particular enter the plasma dispersion in the direction parallel to the magnetic field only. In the perpendicular plane, the plasma is cold and resides in the lowest Landau level.

The QED effects modify the Maxwell equations and make them nonlinear. They introduce additional electric and magnetic susceptibilities of vacuum:

$$\chi_{ij}^{\text{vac}} = -(C_\delta \delta_{ij} - C_\epsilon b_i b_j), \quad (5)$$

$$\eta_{ij}^{\text{vac}} = -(C_\delta \delta_{ij} + C_\mu b_i b_j). \quad (6)$$

Here the coefficients C_δ , C_ϵ , and C_μ are given by complicated functions of B/B_Q presented by Eqs. (28–30) and shown in Fig. 1 in Paper I²². Since the expressions are long and cumbersome, they are not presented here. However, the approximate scalings for both $B \ll B_Q$ and $B \gg B_Q$ are rather simple²². In the weak field limit, $B \ll B_Q$, these quantities take the values

$$C_\delta = (2/45)\alpha(B/B_Q)^2, \quad (7)$$

$$C_\epsilon = (4/45)\alpha(B/B_Q)^2, \quad (8)$$

$$C_\mu = (7/45)\alpha(B/B_Q)^2. \quad (9)$$

In contrast, in the very strong field limit, $B \gg B_Q$, the quantities scale as

$$C_\delta \propto \log(B/B_Q), \quad (10)$$

$$C_\epsilon \propto (B/B_Q), \quad (11)$$

$$C_\mu \sim \text{const.} \quad (12)$$

The total electric permittivity and inverse magnetic permeability are given by equations:

$$\epsilon_{ij} = \delta_{ij} + \chi_{ij}^{\text{vac}} + \chi_{ij}^{\text{plasma}}, \quad (13)$$

$$\mu_{ij}^{-1} = \delta_{ij} + \eta_{ij}^{\text{vac}}. \quad (14)$$

The dispersion relations and polarizations of the plasma waves are found from the wave equation:

$$\left(\frac{\omega^2}{c^2} \epsilon_{il} - e_{ijk} e_{lqr} k_j k_r \mu_{kq}^{-1} \right) \tilde{E}_l = 0 \quad (15)$$

or more explicitly

$$\left[\frac{\omega^2}{c^2} \epsilon_{il} + \mu_{il}^{-1} k^2 - \mu^{-1} (\delta_{il} k^2 - k_i k_l) + \delta_{il} \mu_{jk}^{-1} k_j k_k - \mu_{ij}^{-1} k_j k_l - \mu_{lj}^{-1} k_j k_i \right] \tilde{E}_l = 0, \quad (16)$$

where \tilde{E}_l denotes the fluctuating electric field of a wave, e_{ijk} is the Levi-Civita symbol, $\mu^{-1} \equiv \mu_{ii}^{-1}$ is the trace of μ_{ij}^{-1} , and $k^2 = k_i k_i$.

Equating the determinant of the matrix in the square brackets to zero, we obtain:

$$\begin{aligned} \det & \left[\frac{\omega^2}{c^2} \left(\delta_{ij} + \chi_{ij}^{\text{vac}} + \chi_{ij}^{\text{plasma}} \right) - (\delta_{ij} k^2 - k_i k_j) (1 + \eta^{\text{vac}}) \right. \\ & \left. + \delta_{ij} \eta_{mn}^{\text{vac}} k_m k_n + \eta_{ij}^{\text{vac}} k^2 - (\eta_{im}^{\text{vac}} k_m k_j + \eta_{jm}^{\text{vac}} k_m k_i) \right] = 0, \end{aligned} \quad (17)$$

where $\eta^{\text{vac}} = \eta_{ii}^{\text{vac}}$ is the trace of η_{ij}^{vac} . Upon some algebra, the dispersion equation takes the following form:

$$\det \left[\frac{\omega^2}{c^2} \begin{pmatrix} 1 - C_\delta & 0 & 0 \\ 0 & 1 - C_\delta & 0 \\ 0 & 0 & 1 - C_\delta + C_\epsilon \end{pmatrix} + \frac{\omega^2}{c^2} \begin{pmatrix} \chi_{ij}^{\text{plasma}} \end{pmatrix} \right. \\ \left. - k^2 \begin{pmatrix} \cos^2 \theta (1 - C_\delta) & 0 & \sin \theta \cos \theta (1 - C_\delta) \\ 0 & (1 - C_\delta - C_\mu \sin^2 \theta) & 0 \\ \sin \theta \cos \theta (1 - C_\delta) & 0 & \sin^2 \theta (1 - C_\delta) \end{pmatrix} \right] = 0. \quad (18)$$

In order to proceed further, we need to specify the function Q . If we consider a one-dimensional particle velocity distribution function, we get^{23,25}:

$$Q(\omega, k) = \frac{\omega_p^2}{\omega^2} W(\omega, k_z), \quad (19)$$

where the W function is given by the standard integral:

$$W = -\frac{\omega^2}{k_z} \int_{-c}^c \frac{1}{\omega - k_z v_z + i\nu} \frac{df}{dv_z} dv_z. \quad (20)$$

Here, $\nu \rightarrow +0$ is needed to take into account collisionless Landau damping. The distribution function is typically expressed through the variable $u_z = v_z / \sqrt{1 - v_z^2/c^2}$, so that its normalization takes a simple form:

$$\int_{-\infty}^{\infty} f(u_z) du_z = 1. \quad (21)$$

For simplicity, we consider the one-dimensional Maxwell-Jüttner distribution,

$$f(u_z) = \frac{1}{2cK_1(1/\Theta)} \exp(-\gamma/\Theta), \quad (22)$$

where K_1 is the modified Bessel function of the second kind, $\gamma = 1/\sqrt{1 - v_z^2/c^2} = \sqrt{1 + u_z^2/c^2}$ is the relativistic gamma-factor, and $\Theta = k_B T / (m_e c^2)$ is the temperature parameter. We will consider the ultrarelativistic limit, $\Theta \gg 1$, in which case $K_1(1/\Theta) \approx \Theta$.

The Landau damping is strong when $1 - \omega^2/(k_z^2 c^2) \sim 1/\Theta^2$, which is the condition when the phase velocity of the wave is comparable to the thermal velocities of the particles. In this case, the function Q has a large imaginary part, comparable to its real part. Its imaginary part is relatively small in the following two limiting cases:

$$\left| 1 - \frac{\omega^2}{k_z^2 c^2} \right| \gg \frac{1}{\Theta^2} \quad (\text{Case I}), \quad (23)$$

and

$$\left| 1 - \frac{\omega^2}{k_z^2 c^2} \right| \ll \frac{1}{\Theta^2} \quad (\text{Case II}). \quad (24)$$

As discussed in^{23,25,26}, in Case I, the Q function takes the form

$$Q \approx \frac{\omega_p^2}{\Theta(\omega^2 - k_z^2 c^2)}, \quad (25)$$

while in Case II, we have

$$Q \approx \frac{2\Theta\omega_p^2}{k_z^2 c^2}. \quad (26)$$

Obviously, in the case $\omega^2 \geq k_z^2 c^2$, the imaginary part is absent since the phase velocity of such waves is greater than the speed of light, and they are not affected by Landau damping.

Fig. 1 illustrates the location of regions corresponding to Case I and Case II in the k - ω plane. For concreteness, we assume that a quantity is “much greater” or “much smaller” when it differs by a factor of three. The big light-blue region represents inequality $|1 - \omega^2/k_z^2 c^2| > 3/\Theta^2$, and the narrow orange region represents $|1 - \omega^2/k_z^2 c^2| < 1/3\Theta^2$. The region above the dashed black line is where the waves are superluminal, $\omega^2 \geq k_z^2 c^2$, hence Landau damping is absent. The collisionless damping can be important in the unshaded region below the dashed line, in-between the blue and orange regions. It is seen that Case I dominates the waves’ dispersion, especially in the ultra-relativistic regime, $\Theta \gg 1$.

As in Paper I²², we observe that (i) Eq. (17) contains a common term $(1 - C_\delta)$ and (ii) all plasma susceptibilities χ_{ij} are proportional to ω_p^2 . Therefore, we renormalize the plasma frequency and define new quantities:

$$\omega_p^2 \rightarrow \omega_{p*}^2 \equiv \frac{\omega_p^2}{1 - C_\delta}, \quad \alpha_\epsilon = \frac{C_\epsilon}{1 - C_\delta}, \quad \alpha_\mu = \frac{C_\mu}{1 - C_\delta}. \quad (27)$$

Fig. 2 illustrates the behavior of these parameters as a function of the field strength.

With the above definitions, the dispersion relation is

$$\det \left[\frac{\omega^2}{c^2} \begin{pmatrix} \epsilon_{\perp*} & ig_* & 0 \\ -ig_* & \epsilon_{\perp*} & 0 \\ 0 & 0 & \epsilon_{\parallel*} \end{pmatrix} - k^2 \begin{pmatrix} \cos^2 \theta & 0 & \sin \theta \cos \theta \\ 0 & 1 - \alpha_\mu \sin^2 \theta & 0 \\ \sin \theta \cos \theta & 0 & \sin^2 \theta \end{pmatrix} \right] = 0, \quad (28)$$

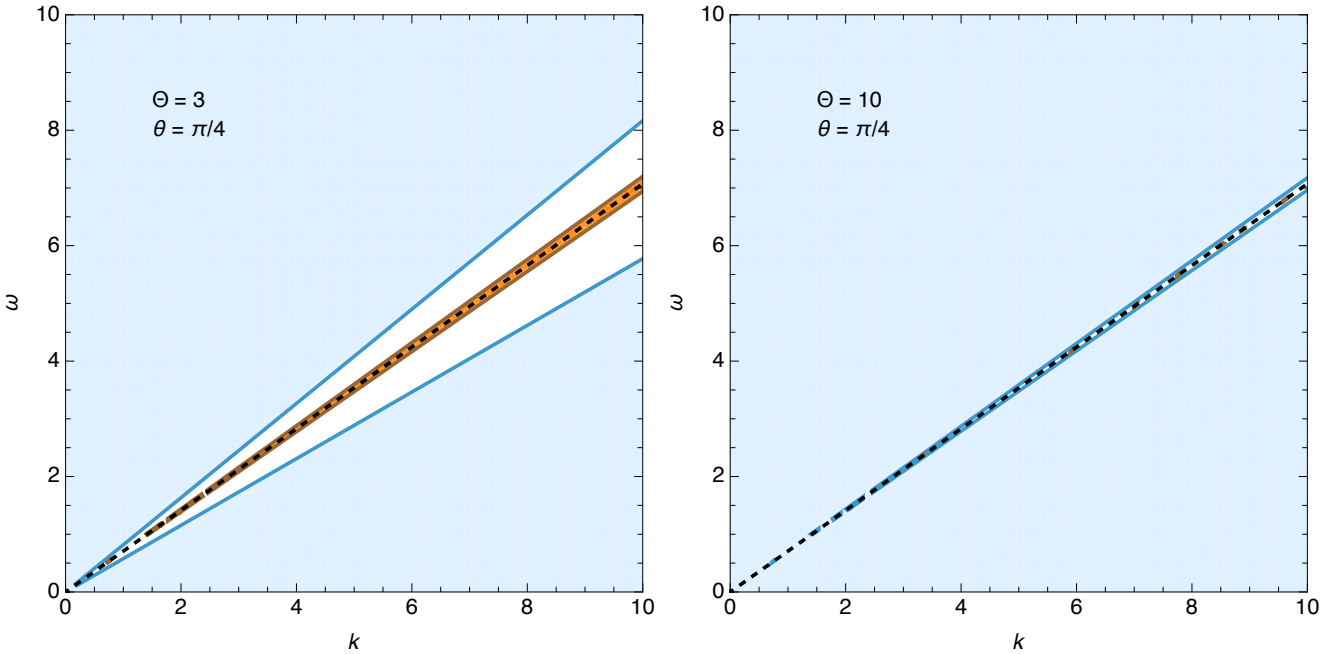


FIG. 1. Regions approximately corresponding to Case I (light-blue) and Case II (orange) are shown for two values of temperature Θ and two propagation angles θ . Above the dashed black line, waves are superluminal and decoupled from Landau damping. The damping can be significant in the unshaded region below the dashed line, in-between the blue and orange regions. Case I dominates waves' dispersion, especially in the ultra-relativistic plasma.

where

$$\epsilon_{\perp*} = 1 - \frac{\omega_{p*}^2}{\omega^2 - \Omega^2}, \quad (29)$$

$$\epsilon_{\parallel*} = 1 + \alpha_{\epsilon} - Q_{*}, \quad (30)$$

$$g_{*} = -\frac{\omega_{p*}^2 \Omega}{\omega(\omega^2 - \Omega^2)} \frac{\Delta n}{n}, \quad (31)$$

$$Q_{*} \approx \begin{cases} \frac{\omega_{p*}^2}{\Theta(\omega^2 - k^2 c^2 \cos^2 \theta)} & \text{(Case I),} \\ \frac{2\Theta\omega_{p*}^2}{k^2 c^2 \cos^2 \theta} & \text{(Case II).} \end{cases} \quad (32)$$

One readily sees that the effect of the quantum vacuum re-

duces to the renormalization of the plasma frequency and addition of two field-dependent coefficients to the dispersion relation, via α_{ϵ} in the ω^2 -term and via α_{μ} in the $\epsilon_{\parallel*}$ component entering the k^2 -term. In a super-critical magnetic field $B \gg B_Q$, the only strong effect is due to α_{ϵ} , which grows linearly with the field strength $\alpha_{\epsilon} \propto B$. It exceeds unity $\alpha_{\epsilon} > 1$ in the field $B/B_Q \gg 1/\alpha \sim 137$. The QED modification to the plasma frequency is small, on the order of a few percent. It grows logarithmically with the field strength $(\omega_{p*} - \omega_p)/\omega_p \simeq C_{\delta} \propto \log B$. The contribution from α_{μ} is always small and saturates $\alpha_{\mu} \sim \text{few} \times 10^{-3}$.

Introducing the index of refraction, $N^2 = k^2 c^2 / \omega^2$, we finally obtain

$$\det \begin{bmatrix} N^2 \cos^2 \theta - \epsilon_{\perp*} & -i g_{*} & N^2 \sin \theta \cos \theta \\ i g_{*} & N^2 (1 - \alpha_{\mu} \sin^2 \theta) - \epsilon_{\perp*} & 0 \\ N^2 \sin \theta \cos \theta & 0 & N^2 \sin^2 \theta - \epsilon_{\parallel*} \end{bmatrix} = 0. \quad (33)$$

Expansion of the determinant yields

$$N^4 A + N^2 B + C = 0, \quad (34)$$

where the scalar coefficients, A , B , C , are

$$A = (\epsilon_{\perp*} \sin^2 \theta + \epsilon_{\parallel*} \cos^2 \theta) (1 - \alpha_{\mu} \sin^2 \theta), \quad (35)$$

$$B = -[\epsilon_{\perp*} \epsilon_{\parallel*} (1 + \cos^2 \theta - \alpha_{\mu} \sin^2 \theta) + (\epsilon_{\perp*}^2 - g_{*}^2) \sin^2 \theta], \quad (36)$$

$$C = \epsilon_{\parallel*} (\epsilon_{\perp*}^2 - g_{*}^2). \quad (37)$$

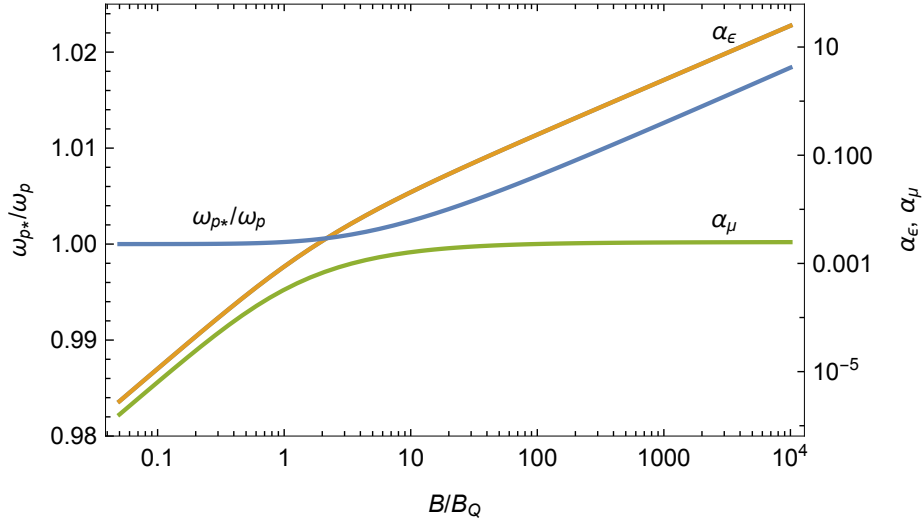


FIG. 2. QED modification of the plasma frequency (log-linear scale, left axis) and quantities $\alpha_\epsilon, \alpha_\mu$ (log-log scale, right axis) as a function of the magnetic field strength B/B_Q .

We use the same letter B for one of the coefficients as for the field strength, hoping this would not cause any confusion. Note that the index of refraction enters $\epsilon_{\parallel*}$ through the temperature-dependent function

$$Q_* \approx \begin{cases} \frac{\omega_{p*}^2}{\Theta\omega^2(1-N^2\cos^2\theta)} & \text{(Case I),} \\ \frac{2\Theta\omega_{p*}^2}{\omega^2N^2\cos^2\theta} & \text{(Case II),} \end{cases} \quad (38)$$

so that Eq. (34) is no longer bi-quadratic. By expanding out $\epsilon_{\parallel*}$, we rearrange the polynomial into the form

$$[N^4\tilde{A} + N^2\tilde{B} + \tilde{C}] + Q_* [N^4A_* + N^2B_* + C_*] = 0 \quad (39)$$

where "starred" quantities are the terms in the coefficients that are proportional to Q_* and "tilded" quantities are those that are not. The tilded coefficients are

$$\tilde{A} = (\epsilon_{\perp*}\sin^2\theta + (1 + \alpha_\epsilon)\cos^2\theta)(1 - \alpha_\mu\sin^2\theta), \quad (40)$$

$$\tilde{B} = -[\epsilon_{\perp*}(1 + \alpha_\epsilon)(1 + \cos^2\theta - \alpha_\mu\sin^2\theta) + (\epsilon_{\perp*}^2 - g_*^2)\sin^2\theta], \quad (41)$$

$$\tilde{C} = (1 + \alpha_\epsilon)(\epsilon_{\perp*}^2 - g_*^2), \quad (42)$$

and the starred coefficients are

$$A_* = -\cos^2\theta(1 - \alpha_\mu\sin^2\theta), \quad (43)$$

$$B_* = \epsilon_{\perp*}(1 + \cos^2\theta - \alpha_\mu\sin^2\theta), \quad (44)$$

$$C_* = -(\epsilon_{\perp*}^2 - g_*^2). \quad (45)$$

As Q_* contains factors of N^2 in the denominator, we can rearrange Eq. (39) into a bi-cubic polynomial

$$\mathcal{A}N^6 + \mathcal{B}N^4 + \mathcal{C}N^2 + \mathcal{D} = 0 \quad (46)$$

where the coefficients are now combinations of tilded and starred quantities depending on the case chosen for Q_* . The coefficients for Case I are listed in Eqs. (47) - (50), while the coefficients for Case II are listed in Eqs. (81) - (84). Thus, the dispersion relation can always be solved in principle using the cubic formula. These solutions are typically algebraically complicated. We now explore simple special cases and limiting behavior.

III. ANALYSIS

A. Case I

In Case I, the coefficients in Eq (46) are

$$\mathcal{A} = -\cos^2\theta \frac{\Theta\omega^2}{\omega_{p*}^2} \tilde{A}, \quad (47)$$

$$\mathcal{B} = \frac{\Theta\omega^2}{\omega_{p*}^2} (\tilde{A} - \cos^2\theta\tilde{B}) + A_*, \quad (48)$$

$$\mathcal{C} = \frac{\Theta\omega^2}{\omega_{p*}^2} (\tilde{B} - \cos^2\theta\tilde{C}) + B_*, \quad (49)$$

$$\mathcal{D} = \frac{\Theta\omega^2}{\omega_{p*}^2} \tilde{C} + C_*. \quad (50)$$

The majority of parameter space is occupied by Case I (Fig. 1), especially in the ultra-relativistic regime. In particular, the asymptotic behavior of the dispersion relation will mainly reside in Case I with the only exceptions being when $\omega \sim k_z$. We present the general behavior in Figs. 3 - 5. Analytic results can be derived for several limiting cases, which we explore now.

1. Resonances

When N^2 diverges, there are frequencies for which ω remains constant as $k \rightarrow \infty$, the resonances. In Case I, $N^2 \rightarrow \infty$ when $\mathcal{A} \rightarrow 0$. This reads

$$-\cos^2 \theta \frac{\Theta \omega^2}{\omega_{p*}^2} \tilde{A} = 0 \quad (51)$$

which reduces to

$$\omega_{\infty}^{(1)} = \sqrt{\Omega^2 + \frac{\sin^2 \theta}{\sin^2 \theta + (1 + \alpha_{\epsilon}) \cos^2 \theta} \omega_{p*}^2}. \quad (52)$$

In parallel propagation, $\theta = 0$, this resonance becomes

$$\omega_{\infty}^{(1)} = \Omega. \quad (53)$$

This branch does *not* appear in this form for perpendicular propagation, for $\theta = \pi/2$. That is a special case that is handled in Section III A 4.

Additional branches still exist when $\mathcal{A} = 0$, which can provide additional resonances. Consider $\mathcal{B} = 0$, which is

$$\frac{\Theta \omega^2}{\omega_{p*}^2} (\tilde{A} - \cos^2 \theta \tilde{B}) + A_* = 0. \quad (54)$$

$\mathcal{A} = 0$ implies $\tilde{A} = 0$, and after some algebra this reduces to

$$\begin{aligned} \epsilon_{\perp*} (1 + \alpha_{\epsilon}) (1 + \cos^2 \theta - \alpha_{\mu} \sin^2 \theta) \\ - \frac{\omega_{p*}^2}{\Theta \omega^2} (1 - \alpha_{\mu} \sin^2 \theta) + (\epsilon_{\perp*}^2 - g_*^2) \sin^2 \theta = 0. \end{aligned} \quad (55)$$

There is also the possibility of $\mathcal{C} = 0$ simultaneously with \mathcal{B} , which adds the condition

$$\begin{aligned} \epsilon_{\perp*} \left(1 + \alpha_{\epsilon} - \frac{\omega_{p*}^2}{\Theta \omega^2} \right) (1 + \cos^2 \theta - \alpha_{\mu} \sin^2 \theta) \\ + (\epsilon_{\perp*}^2 - g_*^2) (\sin^2 \theta + (1 + \alpha_{\epsilon}) \cos^2 \theta) = 0. \end{aligned} \quad (56)$$

Both Eqs. (55) and (56) share similarities with the analogous condition for the cold plasma²², but the extra factor of N^2 in Q_* shuffles around terms between the coefficients. The exact behavior of the remaining resonances is analytically complicated, but are plotted and explored numerically in Figs. (4) and (5).

2. Cutoffs

Where $N^2 < 0$, the index of refraction is imaginary, causing waves to rapidly attenuate. The cutoff frequencies are identified at the boundary $N^2 = 0$. For Case I, this condition is

$$\tilde{C} + \frac{\omega_{p*}^2}{\Theta \omega^2} C_* = 0 \quad (57)$$

which reads

$$\left(1 + \alpha_{\epsilon} - \frac{\omega_{p*}^2}{\Theta \omega^2} \right) (\epsilon_{\perp*}^2 - g_*^2) = 0. \quad (58)$$

This reduces to

$$\omega_0^{(1)} = \frac{\omega_{p*}}{\sqrt{\Theta(1 + \alpha_{\epsilon})}} \quad (59)$$

and

$$\epsilon_{\perp*}^2 - g_*^2 = 0. \quad (60)$$

Eq. (59) is a generalization of the cold plasma result, and Eq. (60) is exactly the cold plasma result²². Eq. (60) has simple limiting cases for $|\Delta n/n| \rightarrow 0$ and $|\Delta n/n| \rightarrow 1$. For $|\Delta n/n| \rightarrow 0$, the cutoff frequencies are

$$\omega_0^{(2)} \approx \frac{\omega_{p*}^2 \Omega}{\omega_{p*}^2 + \Omega^2} \left| \frac{\Delta n}{n} \right|, \quad (61)$$

$$\omega_0^{(3)} \approx \sqrt{\omega_{p*}^2 + \Omega^2}. \quad (62)$$

For $|\Delta n/n| \rightarrow 1$, they are

$$\omega_0^{(2,3)} = \sqrt{\omega_{p*}^2 + \frac{1}{4} \Omega^2} \mp \frac{1}{2} \Omega. \quad (63)$$

3. Parallel Propagation

Setting $\theta = 0$ in Eq. (33) leads directly to three branches. The first corresponds to $\epsilon_{||*} = 0$, which for Case I works out to be

$$N^2 = 1 - \frac{\omega_{p*}^2}{\Theta \omega^2 (1 + \alpha_{\epsilon})}. \quad (64)$$

This is the Langmuir mode branch with dispersion relation

$$\omega^2 = k^2 c^2 + \frac{\omega_{p*}^2}{\Theta (1 + \alpha_{\epsilon})}. \quad (65)$$

The remaining branches are shared between both cases, and are obtained from

$$(N^2 - \epsilon_{\perp*})^2 - g_*^2 = 0, \quad (66)$$

which has solutions

$$N^2 = \epsilon_{\perp*} \pm g_*. \quad (67)$$

This case is similar to the cold plasma of Paper I²².

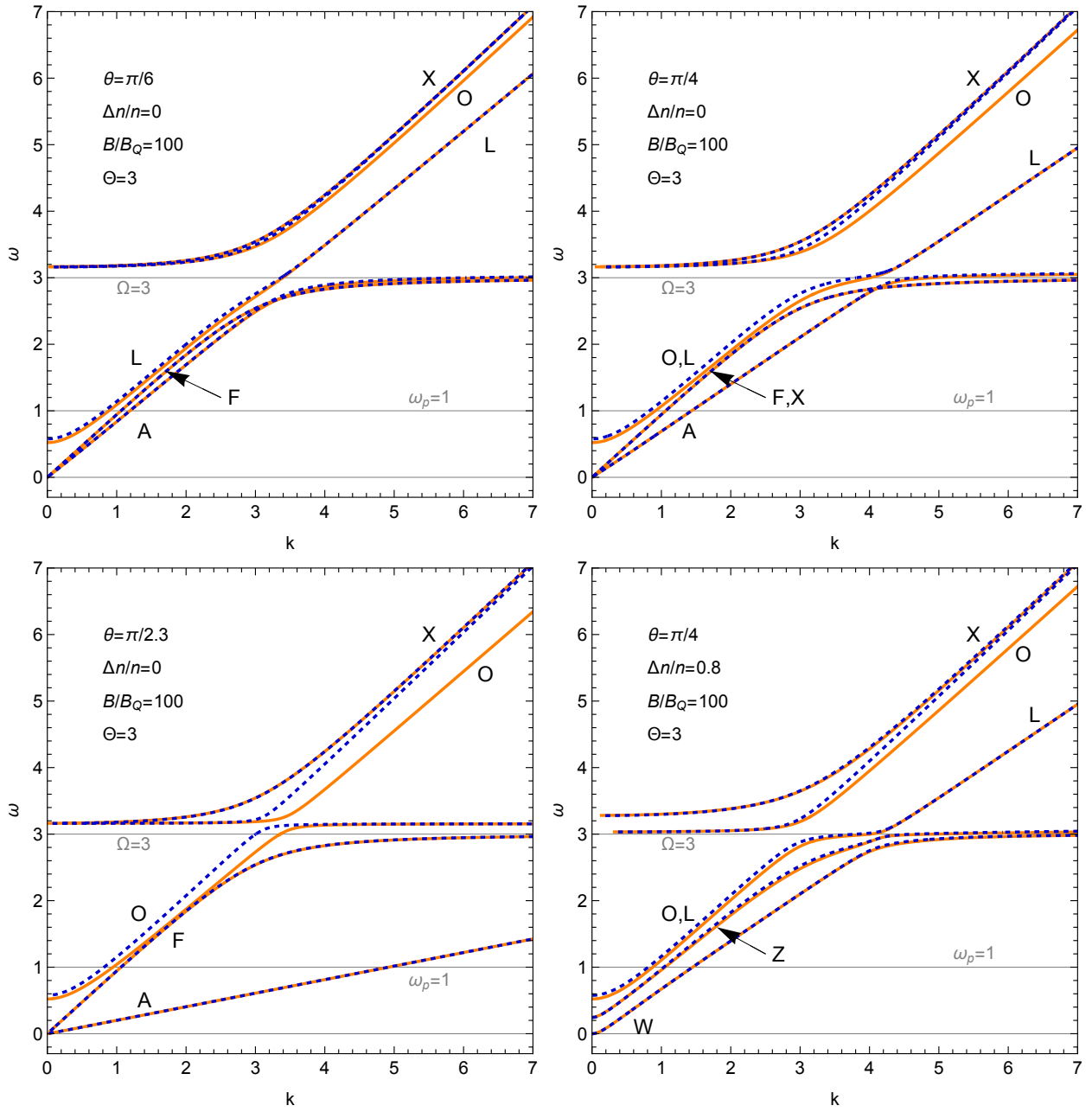


FIG. 3. The schematic representation the plasma dispersion curves $\omega(k)$ for electrically neutral ($\Delta n/n = 0$) and non-neutral ($\Delta n/n = 0.8$) relativistic magnetized plasma. The units are arbitrary, but we set the speed of light to $c = 1$. We set the numerical values of the plasma and cyclotron frequencies to be $\omega_p = 1$, $\Omega = 3$. The temperature parameter is chosen to be $\Theta = 3$ for illustrative purposes only as, formally, $\Theta \gg 1$ in the ultrarelativistic plasma. Both standard (dashed blue curves) and QED-modified with $B/B_Q = 100$ (orange curves) branches of plasma normal modes are shown. The wave branches are labeled as follows: “A”—Alfvén wave, “F”—fast magnetosonic wave, “X”—extraordinary electromagnetic wave, “O”—ordinary electromagnetic wave(in a neutral plasma, it consists of two branches split around the cyclotron frequency), “W”—whistler wave, “Z”—Z-mode (the lower-frequency branch of the extraordinary wave, also called the slow extraordinary mode), “L”—Langmuir mode.

4. Perpendicular Propagation

At $\theta = \pi/2$, Eq. (46) reduces to the bi-quadratic equation

$$N^4 \left(\tilde{A} + \frac{\omega_{p*}^2}{\Theta \omega^2} A_* \right) + N^2 \left(\tilde{B} + \frac{\omega_{p*}^2}{\Theta \omega^2} B_* \right) + \left(\tilde{C} + \frac{\omega_{p*}^2}{\Theta \omega^2} C_* \right) = 0. \quad (68)$$

This is precisely the dispersion equation for the cold plasma case except with $\omega_{p*}^2 \rightarrow \omega_{p*}^2/\Theta$. The resonance frequency in this case is

$$\omega_{\infty}^{(1)} = \sqrt{\frac{\omega_{p*}^2}{\Theta} + \Omega^2}, \quad (69)$$

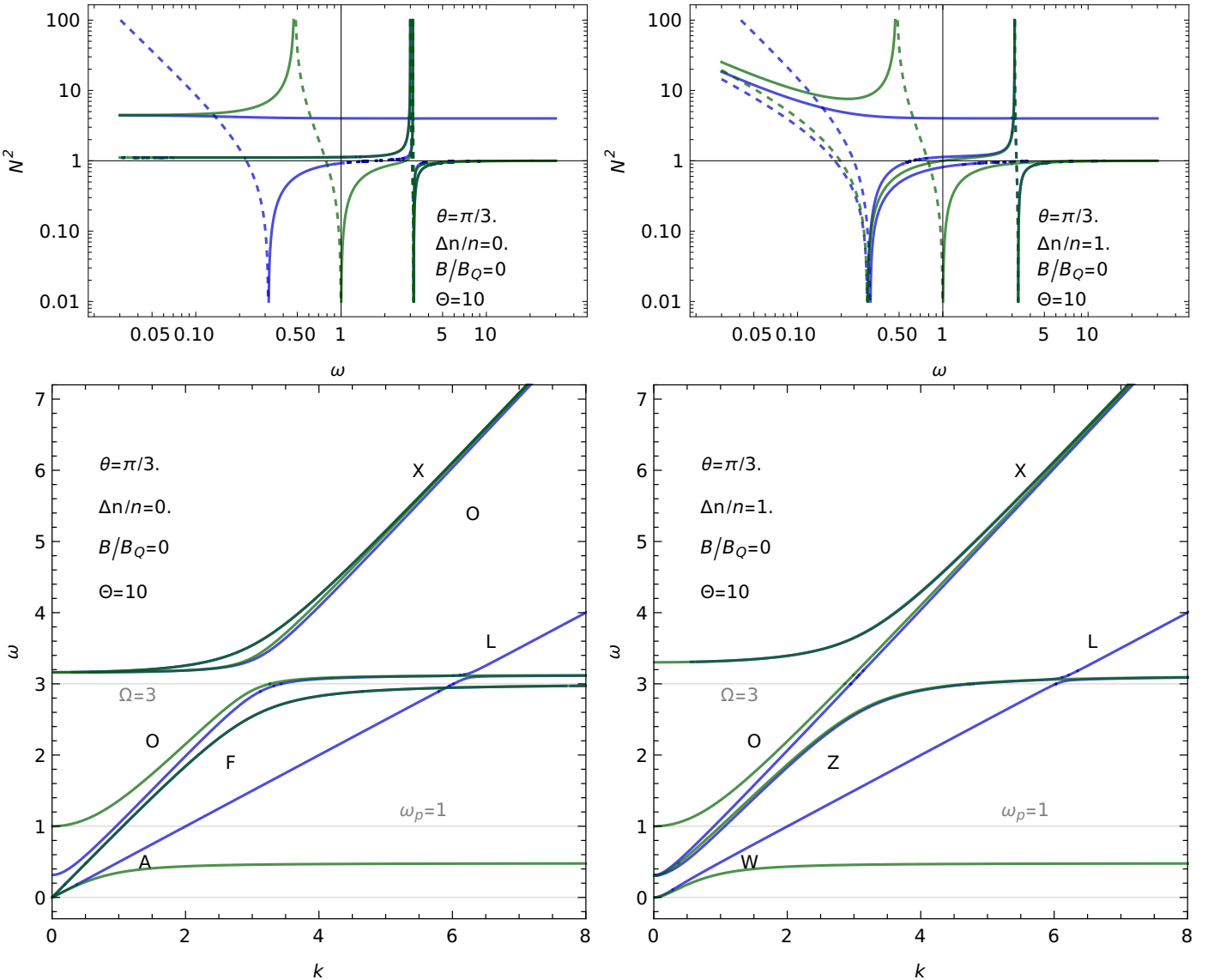


FIG. 4. The schematic representation of the index of refraction squared $N^2(\omega)$ (top row) and the plasma dispersion curves $\omega(k)$ (bottom row) for electrically neutral and non-neutral classical plasmas. The units are arbitrary, but we set the speed of light to $c = 1$. We set the numerical values of the plasma and cyclotron frequencies to be $\omega_p = 1$, $\Omega = 3$, and $\theta = \pi/3$. The cold plasma case is in green, while the thermal plasma case with $\Theta = 10$ is in blue. Both plots are for the non-QED case with $B/B_Q \rightarrow 0$. Solid lines depict propagating waves, i.e., with $N^2 > 0$, and dashed lines depict evanescent branches with $N^2 < 0$. The wave branches are labeled as follows: “A”—Alfvén wave, “F”—fast magnetosonic wave, “X”—extraordinary electromagnetic wave, “O”—ordinary electromagnetic wave (in a neutral plasma, it consists of two branches split around the cyclotron frequency), “W”—whistler wave, “Z”—Z-mode (the lower-frequency branch of the extraordinary wave, also called the slow extraordinary mode), “L”—Langmuir mode.

while the cutoff structure remains the same as the general case discussed above.

5. Low Frequency Asymptotic

The $\omega \rightarrow 0$ behavior is given by taking the approximations

$$\varepsilon_{\perp} \approx 1 + \frac{\omega_p^2}{\Omega^2}, \quad (70)$$

$$g_* \approx \frac{\omega_p^2 \Delta n}{\omega \Omega n}. \quad (71)$$

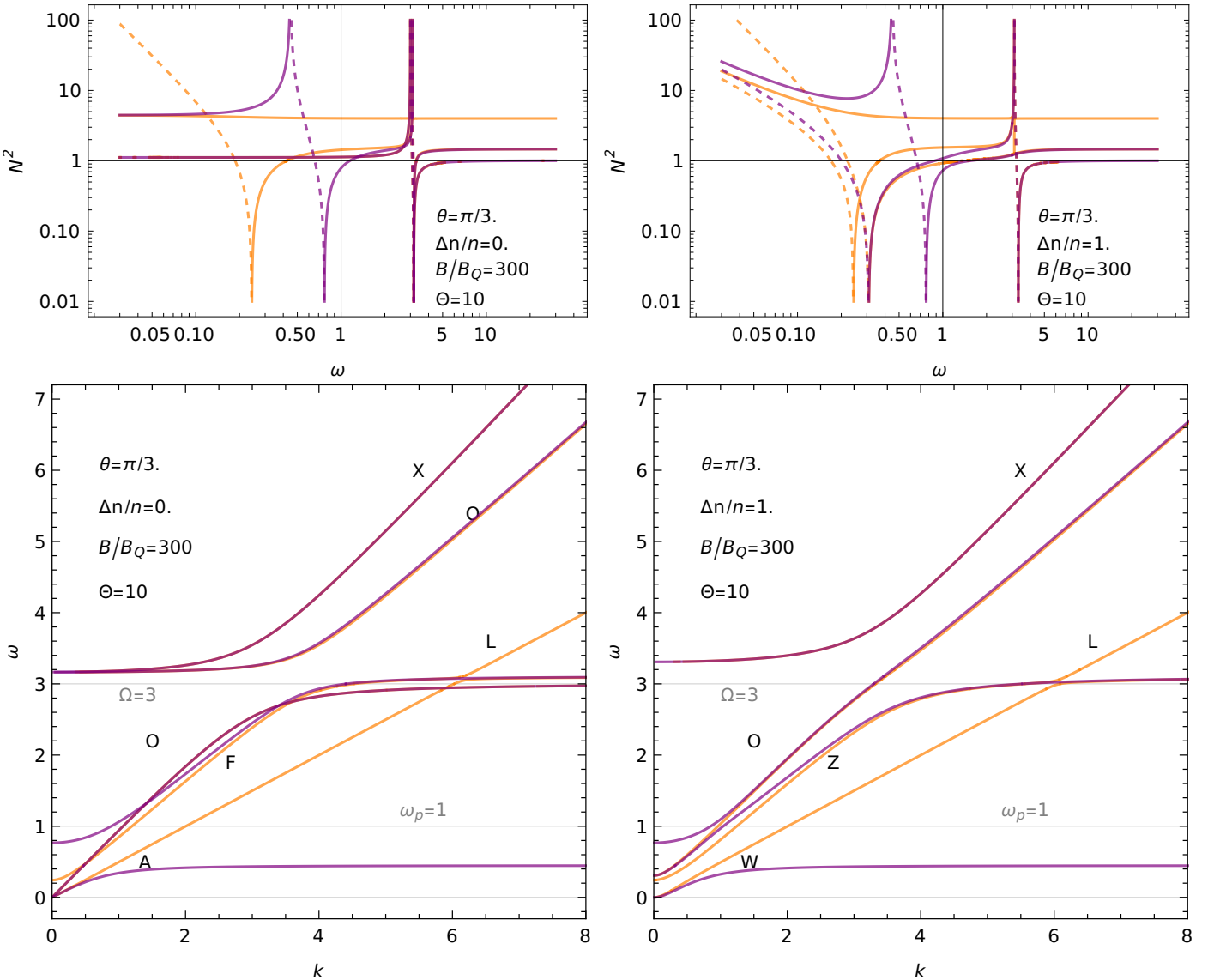


FIG. 5. The schematic representation of the index of refraction squared $N^2(\omega)$ (top row) and the plasma dispersion curves $\omega(k)$ (bottom row) for electrically neutral and non-neutral QED plasmas. The units are arbitrary, but we set the speed of light to $c = 1$. We set the numerical values of the plasma and cyclotron frequencies to be $\omega_p = 1$, $\Omega = 3$, and $\theta = \pi/3$. The wave branches are labeled as in Fig. 4. The cold plasma case is in purple, while the thermal plasma case with $\Theta = 10$ is in orange. Both plots are for the QED case with $B/B_Q = 300$. Solid lines depict propagating waves, i.e., with $N^2 > 0$, and dashed lines depict evanescent branches with $N^2 < 0$.

In the cold plasma case,

$$\epsilon_{\parallel, \text{cold}} = 1 + \alpha_e - \frac{\omega_{p*}^2}{\omega^2}, \quad (72)$$

which becomes large as $\omega \rightarrow 0$ while N^2 remains finite. Because of this, the z polarization in Eq. (33) is small compared to the other polarizations, so the low frequency behavior is determined by the subspace

$$\det \begin{bmatrix} N^2 \cos^2 \theta - \epsilon_{\perp*} & -ig_* \\ ig_* & N^2 (1 - \alpha_\mu \sin^2 \theta) - \epsilon_{\perp*} \end{bmatrix} = 0. \quad (73)$$

In Case I,

$$\epsilon_{\parallel*} = 1 + \alpha_e - \frac{\omega_{p*}^2}{\Theta \omega^2 (1 - N^2 \cos^2 \theta)}, \quad (74)$$

which similarly becomes large as $\omega \rightarrow 0$. Therefore, the same subspace dominates and the cold plasma behavior²² is recovered in this limit. For neutral plasma, this leads to dispersion relations for the Alfvén and fast magnetosonic waves

$$N_+^2 = \frac{1 + \omega_{p*}^2 / \Omega^2}{\cos^2 \theta}, \quad (75)$$

$$N_-^2 = \frac{1 + \omega_{p*}^2 / \Omega^2}{1 - \alpha_\mu \sin^2 \theta}, \quad (76)$$

while for non-neutral plasmas this leads to the whistler wave dispersion relation

$$N^2 = \frac{1}{\cos \theta (1 - \alpha_\mu \sin^2 \theta)} \frac{\omega_{p*}^2 |\Delta n|}{\omega \Omega n}. \quad (77)$$

6. High Frequency Asymptotic

For $\omega \rightarrow \infty$ case, the plasma response is negligible, amounting to taking $\omega_{p*} \rightarrow 0$. This case therefore reduces to the vacuum, no plasma case which is unchanged from the QED vacuum case²². The vacuum dispersion relations are

$$\omega = kc/N_{\perp,\parallel} \quad (78)$$

with

$$N_\perp^2 = \frac{1}{1 - \alpha_\mu \sin^2 \theta}, \quad (79)$$

$$N_\parallel^2 = \frac{1 + \alpha_\epsilon}{1 + \alpha_\epsilon \cos^2 \theta}. \quad (80)$$

The high frequency behavior is shared between both Cases.

B. Case II

In Case II, the coefficients in Eq. (46) are

$$\mathcal{A} = \tilde{A}, \quad (81)$$

$$\mathcal{B} = \tilde{B} + A_*, \quad (82)$$

$$\mathcal{C} = \tilde{C} + B_*, \quad (83)$$

$$\mathcal{D} = C_*. \quad (84)$$

As before, general solutions can be found via the cubic formula and are extremely algebraically complicated. Case II only occupies the thin sliver of (ω, k) space along $\omega \sim k_z$ (Fig. 1), so the general behavior is not typically important especially in cases where $\Theta \gg 1$. In particular, cutoffs and perpendicular propagation *cannot* be considered in Case II due to the singular behavior of Q_* for $\omega \rightarrow 0$ and $\cos^2 \theta \rightarrow 0$. Below, we consider a few simple special cases for the behavior of Case II.

1. Parallel Propagation

Under parallel propagation, $\theta = 0$, there are three branches. Two branches, given by Eq. (67), are shared with Case I. The remaining branch, corresponding to $\epsilon_{\parallel*} = 0$, is

$$N^2 = \frac{2\Theta\omega_{p*}^2}{\omega^2(1 + \alpha_\epsilon)}. \quad (85)$$

2. Neutral Plasma

For a neutral plasma, $\Delta n/n = 0$. Then $g_* = 0$ and Eq. (33) immediately yields three branches. The first branch has dispersion relation

$$N^2 = \frac{\epsilon_{\perp*}}{1 - \alpha_\mu \sin^2 \theta}. \quad (86)$$

The remaining branches are obtained from

$$(N^2 \cos^2 \theta - \epsilon_{\perp*}) (N^2 \sin^2 \theta - \epsilon_{\parallel*}) - (N^2 \sin \theta \cos \theta)^2 = 0. \quad (87)$$

Expanding out $\epsilon_{\parallel*}$ and multiplying through by N^2 yields the bi-quadratic

$$AN^4 + BN^2 + C = 0 \quad (88)$$

with coefficients (not to be confused with the coefficients Eqs. (35) - (37))

$$A = (1 + \alpha_\epsilon) \cos^2 \theta + \epsilon_{\perp*} \sin^2 \theta, \quad (89)$$

$$B = \epsilon_{\perp*} (1 + \alpha_\epsilon) + \frac{2\Theta\omega_{p*}^2}{\omega^2}, \quad (90)$$

$$C = \epsilon_{\perp*} \frac{2\Theta\omega_{p*}^2}{\omega^2 \cos^2 \theta}. \quad (91)$$

The remaining branches are obtained via the quadratic equation, and are algebraically complicated.

3. Low Frequency Asymptotic

In the classical and cold plasma case, $\epsilon_{\parallel*}$ is given by Eq. (72), which becomes large while N^2 remains finite, leading to the reduction of the dispersion matrix to Eq. (73). However, in Case II,

$$\epsilon_{\parallel*} = 1 + \alpha_\epsilon - \frac{2\Theta\omega_{p*}^2}{\omega^2 N^2 \cos^2 \theta}, \quad (92)$$

which remains *finite* as $\omega \rightarrow 0$. As such, in contrast to classical plasmas and Case I, no such simple behavior can be obtained.

4. High Frequency Asymptotic

The high frequency behavior in Case II is identical to that of Case I, which is discussed in Subsection III A 6.

IV. NUMERICAL RESULTS

We present numerical solutions of the full dispersion relation for variations of B , θ , Δn , and Θ . In all figures, dashed lines depict plasma eigenmode branches with $N^2 < 0$, while solid lines depict propagating modes with $N^2 > 0$. The dispersion curves are for Case I only, as the excluded area around

$\omega \sim k_z$ is extremely thin for most values of Θ (see Fig. 1). For illustrative purpose, we chose the numerical values of the plasma and cyclotron frequencies to be $\omega_p = 1$, $\Omega = 3$. We note that in a realistic magnetar magnetosphere, $\omega_p \ll \Omega$ by many orders of magnitude. The units of ω , k are arbitrary, but we set the speed of light $c = 1$.

In all dispersion curve diagrams, the wave branches are labeled as they would be for a classical plasma: "A" is the Alfvén wave, "F" is the fast magnetosonic wave, "X" is the extraordinary oblique electromagnetic wave, "O" is the ordinary oblique electromagnetic wave, "W" is the whistler wave, "Z" is the Z-mode, and "L" is the Langmuir mode.

Fig. 3 helps us with identification of individual branches of the normal plasma modes. Such an identification is fairly straightforward in the case of a quasi-parallel and a quasi-perpendicular propagation.

In the quasi-parallel propagation case (top left panel), we have two modes at low frequencies, both have a linear dispersion, $\omega \propto k$. The upper one is the fast mode (F) and the lower one is the Alfvén (A) mode. Obviously, the Alfvén is slower at oblique angles because its phase speed depends on k_{\parallel} . Next, there is the longitudinal electrostatic Langmuir mode (L), starting at the plasma frequency cutoff (modified by temperature and QED effects) and extending to high frequencies with the linear dispersion proportional to k_{\parallel} . Being a longitudinal mode, it experiences no cyclotron resonance around $\omega \sim \Omega$, but it is generally heavily Landau damped. In contrast, both electromagnetic modes propagating almost along the background field do experience cyclotron resonance in the pair plasma. The electromagnetic mode which has a component of its electric field along the background magnetic field is strongly affected by the QED-strength magnetic field. Namely, $N_{\parallel} > N_{\perp}$ in the QED regime, see Eqs. (79), (80). This fact easily distinguishes the parallel polarization, which at large angles becomes the ordinary (O) mode. The second mode has the wave electric field orthogonal to the background field, so this polarization corresponds to the extraordinary (X) mode at large angles. The fast mode can be viewed as the lower-frequency (i.e., below the cyclotron resonance) extension of the X mode.

In the quasi-perpendicular propagation case (bottom left panel), one can readily identify the O mode which experiences a sharp cyclotron resonance and which phase velocity strongly depends on the strength of the ambient magnetic field (compare solid orange and dashed blue curves). Similarly, we identify the X mode above the resonance and below the resonance, where it is labeled as the F mode. The Alfvén mode is clearly seen by its linear dispersion and low phase speed, whereas the Langmuir branch falls outside of the plotting box.

Identification of the modes at oblique angles (top right panel) may be somewhat perplexing. Still, the O, X and L modes above the cyclotron resonance are easily identifiable by their high- ω , high- k asymptotics. Similarly, the F (same as X) and A modes below the plasma frequency are well observed by their low- ω , low- k linear dispersion. At intermediate frequencies, one observes that the O mode is electromagnetically coupled to the non-quasi-neutral L mode.

Finally, transitioning from the electrically neutral to the

non-neutral plasma (bottom right panel), one observes that the low-frequency branches undergo modifications. The A mode exhibits a whistler-like quadratic dispersion, $\omega \propto kk_{\parallel}$, and is consequently labeled as W. The F mode transforms into the Z mode, characterized by a distinct new cutoff frequency that asymptotically approaches the plasma cutoff when $|\Delta n/n|$ approaches unity.

A. Classical Plasma: Thermal Effects

The index of refraction $N^2(\omega)$ and dispersion curves $\omega(k)$ in a non-QED cold and thermal plasma are shown in Fig. 4. The cold case is plotted in green, while the thermal case is plotted in blue. The figure displays the mode structure for cold and thermal plasma in a very weak field, $B \ll B_Q$, for which quantum effects are negligible. For illustrative purposes, we chose the propagation angle $\theta = \pi/3$ and numerical values of the plasma and cyclotron frequencies to be $\omega_p = 1$ and $\Omega = 3$ respectively. For the thermal plasma, we chose temperature parameter $\Theta = 10$. This is for illustrative purposes, as the ultrarelativistic regime is for $\Theta \gg 1$.

Besides the obvious change in mode structure – the propagation of the Alfvén mode and the appearance of the Langmuir mode – thermal effects are not very significant, appearing only in the behavior near the plasma frequency cutoff.

B. QED Plasma: Dependence on magnetic field and propagation angle

For both neutral and non-neutral plasma, the QED effects are largely the same between the cold and thermal plasma cases. This is most plainly seen in Fig. 5, where we plot dispersion curves for the cold and thermal cases in the QED regime. The cold case is plotted in purple, and the thermal case is plotted in orange. The dispersion curves for most of the modes lie on top of each other between the cold and thermal cases. The main differences appear as $\omega \rightarrow 0$, where $\omega_0^{(1)}$ is further reduced from the cold plasma case.

In Fig. 6, we present the dispersion curves (solid orange lines) for an electrically neutral plasma, $\Delta n = 0$, in super-strong B -field of strengths $10^2 \leq B/B_Q \leq 10^4$ for various angles of propagation. The dispersion curves for a non-QED plasma, that is with $B/B_Q \rightarrow 0$, are shown in blue dashed curves for comparison. Similar results are presented for non-neutral plasma in Fig. 7.

For perpendicular propagation, the system reduces to the cold plasma behavior except with $\omega_{p*}^2 \rightarrow \omega_{p*}^2/\Theta$. In particular, the O-mode has no cyclotron resonance and is appreciably slowed by QED effects while the X- and fast modes are not appreciably affected.

The main QED effect, much like in the cold plasma case, is the slowing and angle dependence of the O-mode.

C. QED Plasma: Dependence on temperature and non-neutrality

In Fig. 8, we present the dispersion curves for $B = 300B_Q$, $\theta = \pi/3$ while we vary $\Delta n = 0, 0.5, 1$ and $\Theta = 3, 10, 100, 1000$. The case $\Theta = 3$ is for illustrative purposes only as it does not lie within the ultrarelativistic regime, $\Theta \gg 1$. As discussed in Sec. III, the cutoff frequency $\omega_0^{(1)}$ scales with temperature as $\Theta^{-1/2}$, so the main effect of increasing Θ is $\omega_0^{(1)} \rightarrow 0$. The mode structure otherwise remains relatively unchanged by increasing Θ .

Non-neutrality changes the mode structure similarly to the cold plasma case: the O-mode becomes non-resonant near the cyclotron frequency as $|\Delta n/n| \rightarrow 1$ while the associated cutoff, $\omega_0^{(1)}$, is unaffected by non-neutrality.

V. SUMMARY

Utilizing the QED-plasma framework, we have derived dispersion relations of normal modes in a non-neutral ultrarelativistic pair plasma that is embedded in a QED-strong background magnetic field. We obtained the following results, summarized in Fig. 9.

1. Many effects from the cold plasma presented in Paper I²² are retained. In particular the retention of the classical plasma mode structure (no novel, QED-only modes appearing), the renormalization of the plasma frequency (see Eq. 27, Fig. 2)

$$\omega_{p*} = \frac{\omega_p}{(1 - C_\delta)}, \quad (93)$$

and the entrance of QED corrections via α_e and α_μ .

2. In a QED plasma, increasing B -field strength allows the O-mode to propagate at frequencies below the plasma frequency. Thermal effects further enhance this effect, as seen in Eq. (59),

$$\omega_0^{(1)} = \frac{\omega_{p*}}{\sqrt{\Theta(1 + \alpha_e)}}. \quad (94)$$

3. Similar to the cold plasma case, the ordinary mode is slowed as seen in the increase of the index of refraction, Eq. 80. At high frequencies, $\omega \gg \omega_p$ it has the QED vacuum dispersion relation

$$\omega = kc \sqrt{\frac{1 + \alpha_e \cos^2 \theta}{1 + \alpha_e}}. \quad (95)$$

This effect is independent of the temperature.

We summarize our results in Fig. 9. We plot the plasma dispersion curves (solid orange) for a charge-neutral, thermal QED plasma with $B \sim 10^{17}$ G for oblique propagation, $\theta = \pi/4$. This is compared to the non-QED plasma modes (dashed blue) with minimal thermal effects, i.e. with $B/B_Q \rightarrow$

0 and $\Theta = 1$. Labeled are the Alfvén (A), fast magnetosonic (F), Langmuir (L), ordinary (O), and extraordinary (X) modes. We set the plasma frequency $\omega_p = 1$ and cyclotron frequency $\Omega = 3$.

These results are of particular importance for neutron star and magnetar magnetospheres. The would help one better understand radiation propagation through these environments, including the origin of FRBs, better constrain nuclear equation of state via more accurate X-ray hot-spot reconstruction in pulsars, and more.

ACKNOWLEDGMENTS

This research was supported by the National Science Foundation under Grant PHY-2409249.

1. Bromage, S.-W. Bahk, I. A. Begishev, C. Dorrer, M. J. Guardalben, B. N. Hoffman, J. Oliver, R. G. Roides, E. M. Schiesser, M. J. Shoup III, and et al., “Technology development for ultraintense all-optical systems,” *High Power Laser Science and Engineering* **7**, e4 (2019).
2. C. N. Danson, C. Haefner, J. Bromage, T. Butcher, J.-C. F. Chanteloup, E. A. Chowdhury, A. Galvanauskas, L. A. Gizzi, J. Hein, D. I. Hillier, and et al., “Petawatt and exawatt class lasers worldwide,” *High Power Laser Science and Engineering* **7**, e54 (2019).
3. M. Borysova and on behalf of LUXE, “Studies of high-field QED with the LUXE experiment at the European XFEL,” *Journal of Instrumentation* **16**, C12030 (2021).
4. P. Zhang, S. S. Bulanov, D. Seipt, A. V. Arefiev, and A. G. R. Thomas, “Relativistic plasma physics in supercritical fields,” *Physics of Plasmas* **27**, 050601 (2020), arXiv:2001.00957 [physics.plasm-ph].
5. V. M. Kaspi and A. M. Beloborodov, “Magnetars,” *Ann. Rev. Astron. Astrophys.* **55**, 261–301 (2017), arXiv:1703.00068 [astro-ph.HE].
6. H. Euler, “Über die Streuung von Licht an Licht nach der Diracschen Theorie,” *Annalen der Physik* **418**, 398–448 (1936).
7. S. L. Adler, J. N. Bahcall, C. G. Callan, and M. N. Rosenbluth, “Photon Splitting in a Strong Magnetic Field,” *Phys. Rev. Lett.* **25**, 1061–1065 (1970).
8. V. B. Berestetskii, E. M. Lifshitz, and V. B. Pitaevskii, *Relativistic quantum theory. Pt. 2* (1974).
9. W. Dittrich and H. Gies, *Probing the Quantum Vacuum* (2000).
10. A. K. Harding and D. Lai, “Physics of strongly magnetized neutron stars,” *Reports on Progress in Physics* **69**, 2631–2708 (2006), arXiv:astro-ph/0606674 [astro-ph].
11. A. Y. Potekhin, D. Lai, G. Chabrier, and W. C. G. Ho, “Electromagnetic Polarization in Partially Ionized Plasmas with Strong Magnetic Fields and Neutron Star Atmosphere Models,” *Astrophys. J.* **612**, 1034–1043 (2004), arXiv:astro-ph/0405383 [astro-ph].
12. T. Grismayer, R. Torres, P. Carneiro, F. Cruz, R. Fonseca, and L. O. Silva, “Quantum Electrodynamics vacuum polarization solver,” arXiv e-prints, arXiv:1607.04224 (2016), arXiv:1607.04224 [physics.plasm-ph].
13. T. Grismayer, M. Vranic, J. L. Martins, R. A. Fonseca, and L. O. Silva, “Seeded QED cascades in counterpropagating laser pulses,” *Phys. Rev. E* **95**, 023210 (2017).
14. K. M. Schoeffler, T. Grismayer, D. Uzdensky, R. A. Fonseca, and L. O. Silva, “Bright Gamma-Ray Flares Powered by Magnetic Reconnection in QED-strength Magnetic Fields,” *Astrophys. J.* **870**, 49 (2019), arXiv:1807.09750 [astro-ph.HE].
15. K. M. Schoeffler, T. Grismayer, D. Uzdensky, and L. O. Silva, “High-energy synchrotron flares powered by strongly radiative relativistic magnetic reconnection: 2D and 3D PIC simulations,” *Mon. Not. R. Astron. Soc.* **523**, 3812–3839 (2023), arXiv:2303.16643 [astro-ph.HE].
16. M. Alawashra, J. Benáček, M. Pohl, and M. V. Medvedev, “Electromagnetic field solver for QED polarization in super-strong magnetic fields of magnetars and laser plasmas,” *Physics of Plasmas* **32**, 113903 (2025), arXiv:2503.14387 [physics.plasm-ph].

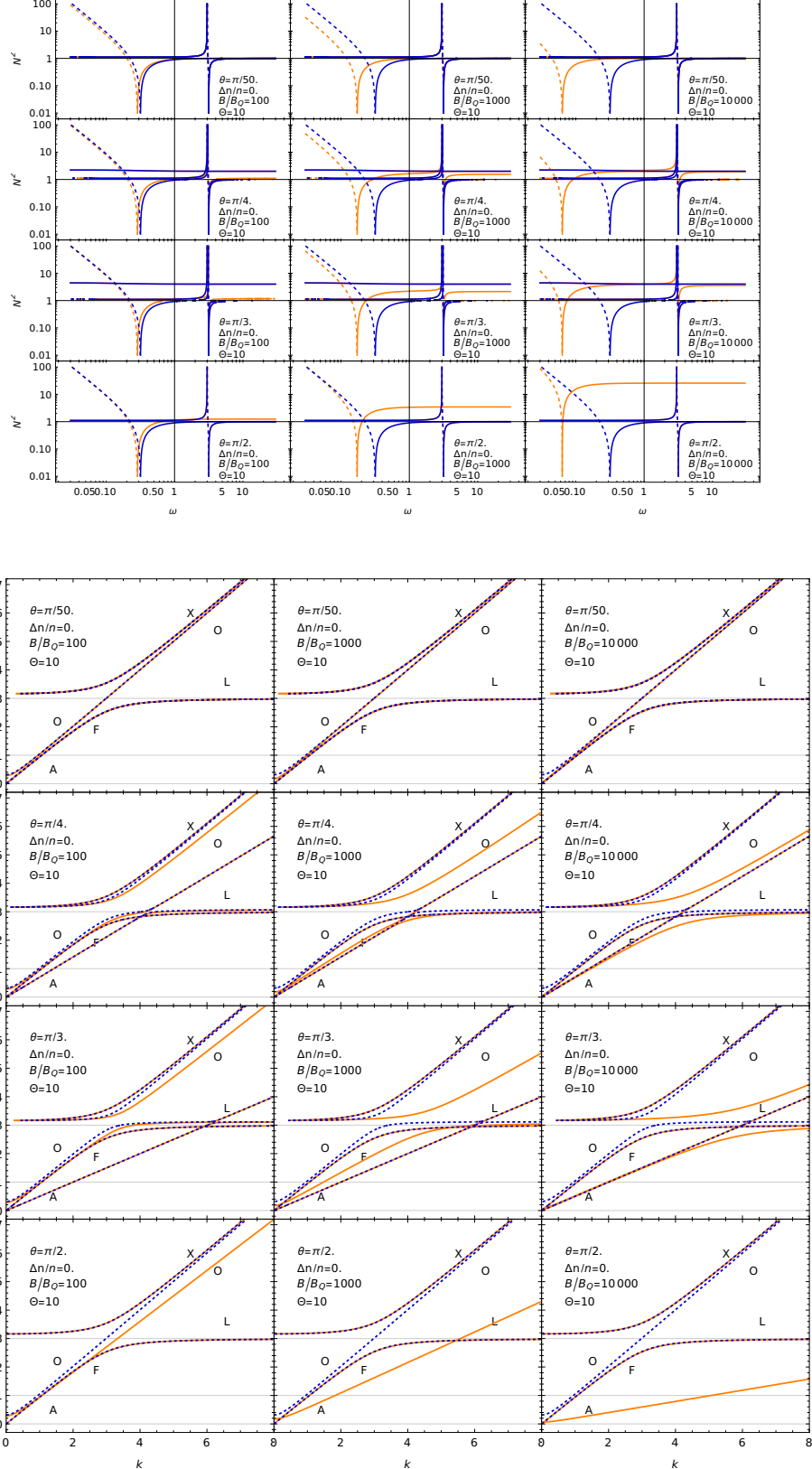


FIG. 6. The index of refraction squared $N^2(\omega)$ (top row) and the plasma dispersion curves $\omega(k)$ (bottom row) for the electrically neutral, $\Delta n/n = 0$, QED plasma as functions of the magnetic field B , and the angle of propagation, θ , with nearly parallel, oblique and perpendicular propagation. The mode structure for perpendicular propagation, $\theta = \pi/2$, is qualitatively different from the general case since it reduces to the cold plasma case²². The blue curves illustrate the non-QED regime and are shown for comparison. The temperature parameter is $\Theta = 10$. The plasma frequency is $\omega_p = 1$ and the cyclotron frequency is $\Omega = 3$. The latter is set to a constant, despite varying B , for the ease of comparison. The wave branches are labeled as in Fig. 4.

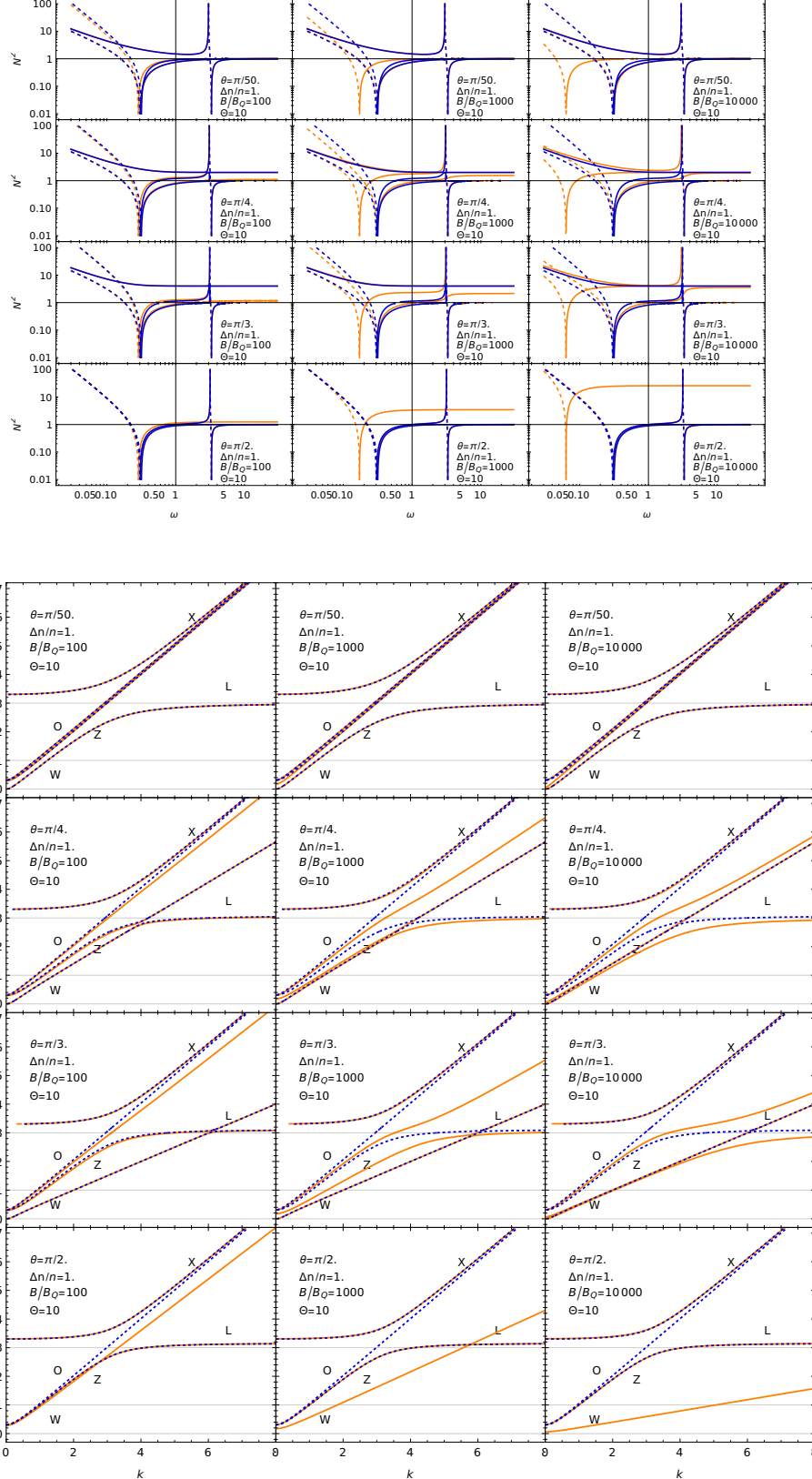


FIG. 7. The index of refraction squared $N^2(\omega)$ (top row) and the plasma dispersion curves $\omega(k)$ (bottom row) for the electrically non-neutral, $\Delta n/n = 1$, QED plasma as functions of the magnetic field B , and the angle of propagation, θ , with nearly parallel, oblique and perpendicular propagation. The mode structure for perpendicular propagation, $\theta = \pi/2$, is qualitatively different from the general case since it reduces to the cold plasma case²². The blue curves illustrate the non-QED regime and are shown for comparison. The temperature parameter is $\Theta = 10$. The plasma frequency is $\omega_p = 1$ and the cyclotron frequency is $\Omega = 3$. The latter is set to a constant, despite varying B , for the ease of comparison. The wave branches are labeled as in Fig. 4.

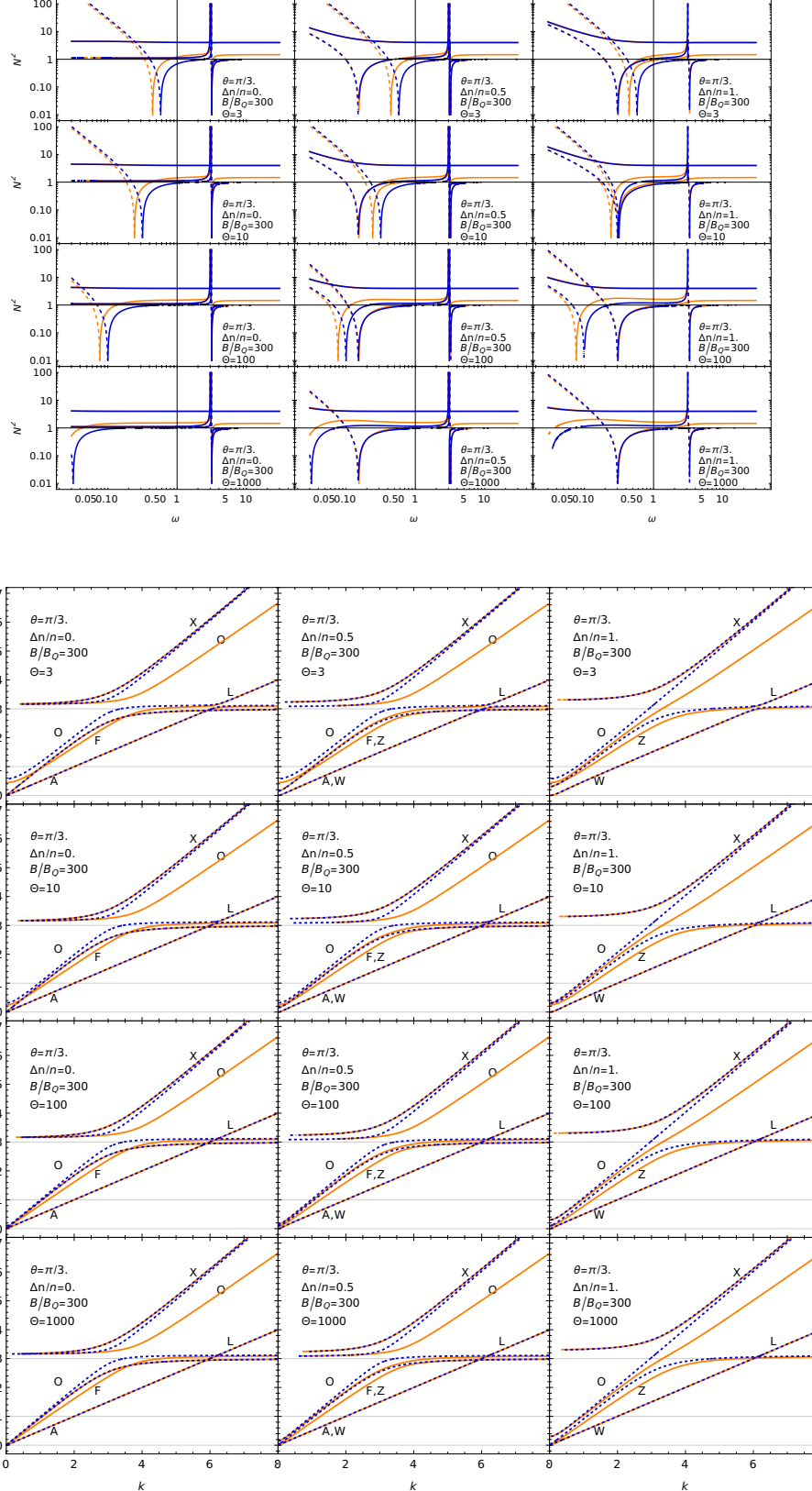


FIG. 8. The index of refraction squared $N^2(\omega)$ (top row) and the plasma dispersion curves $\omega(k)$ (bottom row) as a function of the non-neutrality parameter, $\Delta n/n$, and the temperature parameter Θ . The $\Theta = 3$ case is for illustrative purposes only since it is not within the ultrarelativistic limit $\Theta \gg 1$. The plasma is in the QED regime with $B/B_Q = 300$ and $\theta = \pi/3$. The blue curves illustrate the non-QED regime and are shown for comparison. The plasma frequency is $\omega_p = 1$ and the cyclotron frequency is $\Omega = 3$. The latter is set to a constant, despite varying B , for the ease of comparison. The wave branches are labeled as in Fig. 4.

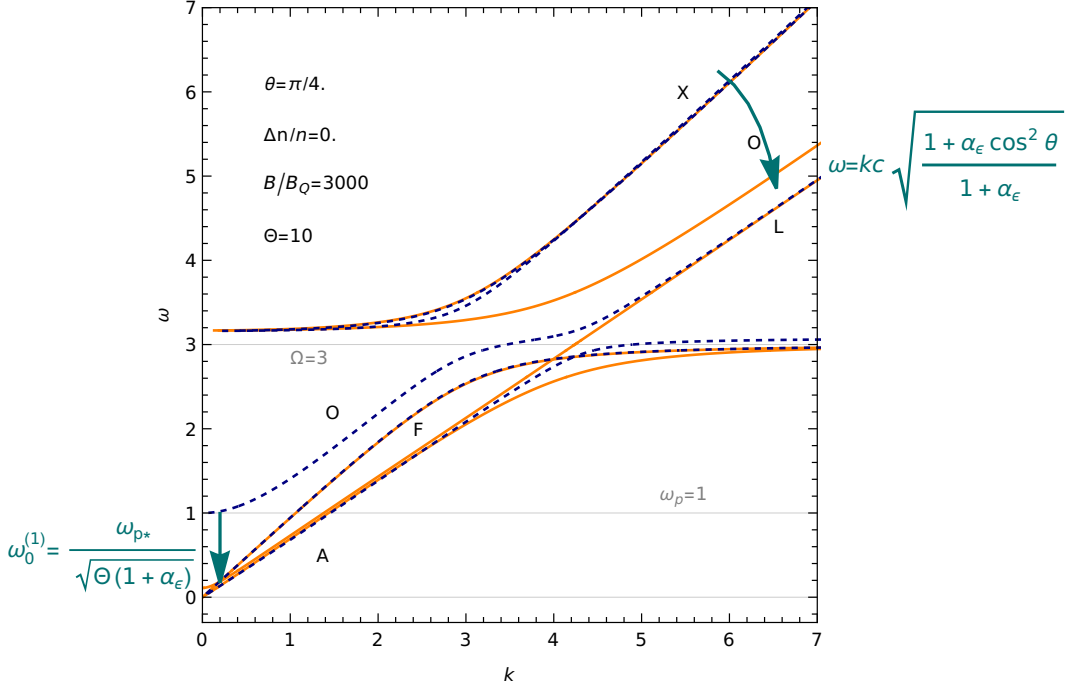


FIG. 9. Summary figure of plasma dispersion curves $\omega(k)$, showing QED effects on charge-neutral, $\Delta n = 0$, thermal plasma. We set $B = 3000B_0 \sim 10^{17}$ G, $\theta = \pi/4$, and $\Theta = k_B T / (m_e c^2) = 10$. The plasma frequency is $\omega_p = 1$ and the cyclotron frequency is $\Omega = 3$. For comparison, dashed blue curves represent the dispersion curves in a non-QED plasma with minimal thermal effects, i.e. for $B/B_Q \rightarrow 0$ and $\Theta = 1$. The wave branches are labeled as follows: “A”—Alfvén wave, “F”—fast magnetosonic wave, “X”—extraordinary electromagnetic wave, “O”—ordinary electromagnetic wave (in a neutral plasma, it consists of two branches split around the cyclotron frequency), “L”—Langmuir mode. The most pronounced QED effects are shown by arrows. They are: (i) the B -field induced transparency of the O-mode seen in the reduced wave cutoff frequency, $\omega_0^{(1)}$ as $k \rightarrow 0$ and (ii) the reduction of the phase speed of the O-mode at $\omega \gg \omega_{p*}$. Thermal effects are also present. Resonant and cutoff frequencies typically scale as $\Theta^{-1/2}$, in this case driving $\omega_0^{(1)}$ even further towards zero and the other resonances towards the cyclotron resonance.

¹⁷E. Liang, T. Clarke, A. Henderson, W. Fu, W. Lo, D. Taylor, P. Chaguine, S. Zhou, Y. Hua, X. Cen, X. Wang, J. Kao, H. Hasson, G. Dyer, K. Serratto, N. Riley, M. Donovan, and T. Ditmire, “High e+/e- Ratio Dense Pair Creation with 10^{21} W.cm⁻² Laser Irradiating Solid Targets,” *Scientific Reports* **5**, 13968 (2015).

¹⁸Y. He, T. G. Blackburn, T. Toncian, and A. V. Arefiev, “Dominance of $\gamma\gamma$ electron-positron pair creation in a plasma driven by high-intensity lasers,” *Communications Physics* **4**, 139 (2021), arXiv:2010.14583 [physics.plasm-ph].

¹⁹A. M. Beloborodov and C. Thompson, “Corona of Magnetars,” *Astrophys. J.* **657**, 967–993 (2007), arXiv:astro-ph/0602417 [astro-ph].

²⁰J. M. Pearson, S. Goriely, and N. Chamel, “Properties of the outer crust of neutron stars from Hartree-Fock-Bogoliubov mass models,” *Phys. Rev. C* **83**, 065810 (2011).

²¹A. Y. Potekhin, A. F. Fantina, N. Chamel, J. M. Pearson, and S. Goriely, “Analytical representations of unified equations of state for neutron-star

matter,” *Astron. & Astrophys.* **560**, A48 (2013), arXiv:1310.0049 [astro-ph.SR].

²²M. V. Medvedev, “Plasma modes in QED super-strong magnetic fields of magnetars and laser plasmas,” *Physics of Plasmas* **30**, 092112 (2023), arXiv:2309.07316 [physics.plasm-ph].

²³M. Gedalin, D. B. Melrose, and E. Gruman, “Long waves in a relativistic pair plasma in a strong magnetic field,” *Phys. Rev. E* **57**, 3399–3410 (1998).

²⁴M. Gedalin, E. Gruman, and D. B. Melrose, “Low-frequency waves in asymmetric magnetized relativistic pair plasma,” *Mon. Not. R. Astron. Soc.* **325**, 715–725 (2001).

²⁵C. Vega, S. Boldyrev, and V. Roytershteyn, “Relativistic Alfvén Turbulence at Kinetic Scales,” *Astrophys. J.* **965**, 27 (2024), arXiv:2402.16218 [physics.plasm-ph].

²⁶B. B. Godfrey, B. S. Newberger, and K. A. Taggart, “A relativistic plasma dispersion function,” *IEEE Transactions on Plasma Science* **3**, 60–67 (1975).